Author Manuscript

Author Manuscript

Author Manuscript

Author Manuscript

HHS Public Access

Author manuscript

*J Mol Cell Cardiol*. Author manuscript; available in PMC 2024 June 01.

Published in final edited form as:

*J Mol Cell Cardiol*. 2023 June ; 179: 30–41. doi:10.1016/j.yjmcc.2023.03.016.

# Btg1 and Btg2 regulate neonatal cardiomyocyte cell cycle arrest

**Nivedhitha Velayutham**[1,2], **Maria Uscategui Calderon**[1,2], **Christina M. Alfieri**[2], **Stephanie L. Padula**[2], **Frank N. van Leeuwen**[3], **Blanca Scheijen**[4], **Katherine E. Yutzey**[1,2,5,*]

[1]Molecular and Developmental Biology Graduate Program, Division of Developmental Biology, Cincinnati Children's Hospital Medical Center, University of Cincinnati College of Medicine, Cincinnati, OH, USA.

[2]The Heart Institute, Division of Molecular Cardiovascular Biology, Cincinnati Children's Hospital Medical Center, Cincinnati, OH, USA.

[3]Princess Máxima Center for Pediatric Oncology, Utrecht, Netherlands.

[4]Radboud University Medical Center, Nijmegen, Netherlands.

[5]Department of Pediatrics, University of Cincinnati College of Medicine, Cincinnati, OH, USA.

## Abstract

Rodent cardiomyocytes undergo mitotic arrest in the first postnatal week. Here, we investigate the role of transcriptional co-regulator Btg2 (B-cell translocation gene 2) and functionally-similar homolog Btg1 in postnatal cardiomyocyte cell cycling and maturation. Btg1 and Btg2 (Btg1/2) are expressed in neonatal C57BL/6 mouse left ventricles coincident with cardiomyocyte cell cycle arrest. Btg1/2 constitutive double knockout (DKO) mouse hearts exhibit increased pHH3+ mitotic cardiomyocytes compared to Wildtype at postnatal day (P)7, but not at P30. Similarly, neonatal AAV9-mediated Btg1/2 double knockdown (DKD) mouse hearts exhibit increased EdU+ mitotic cardiomyocytes compared to Scramble AAV9-shRNA controls at P7, but not at P14. In neonatal rat ventricular myocyte (NRVM) cultures, siRNA-mediated Btg1/2 single and double knockdown cohorts showed increased EdU+ cardiomyocytes compared to Scramble siRNA controls, without increase in binucleation or nuclear DNA content. RNAseq analyses of Btg1/2-depleted NRVMs support a role for Btg1/2 in inhibiting cell proliferation, and in modulating reactive oxygen species response pathways, implicated in neonatal cardiomyocyte cell cycle arrest. Together, these data identify Btg1 and Btg2 as novel contributing factors in mammalian cardiomyocyte cell cycle arrest after birth.

## Graphical Abstract

*Correspondence to Katherine E. Yutzey, PhD, Division of Molecular Cardiovascular Biology, Cincinnati Children's Medical Center ML7020, 240 Albert Sabin Way, Cincinnati, OH 45229, Katherine.Yutzey@cchmc.org, Phone: +1 513-636-8340.

AUTHOR CONTRIBUTIONS

Overall study conceptualization was by NV and KEY. Experimental procedures and data acquisition were performed by NV, MUC, CMA, and SLP. Btg1/2 constitutive knockout mice were provided by FNVL and BS. Data analysis, results interpretation, and manuscript preparation were done by NV and KEY, with comments and approval of MUC, CMA, SLP, FNVL, and BS.

**Publisher's Disclaimer:** This is a PDF file of an unedited manuscript that has been accepted for publication. As a service to our customers we are providing this early version of the manuscript. The manuscript will undergo copyediting, typesetting, and review of the resulting proof before it is published in its final form. Please note that during the production process errors may be discovered which could affect the content, and all legal disclaimers that apply to the journal pertain.

Author Manuscript Author Manuscript Author Manuscript Author Manuscript

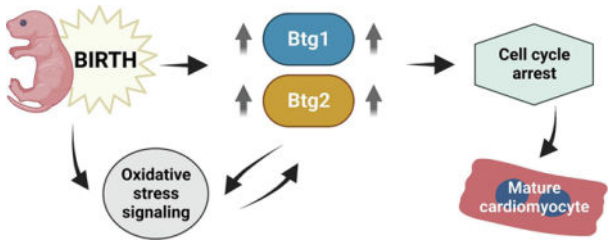


**Keywords**

Neonatal heart development; Cardiomyocyte mitotic arrest; Cardiac cell cycle regulation; Btg1; Btg2

## 1. INTRODUCTION

In adult mammals, including humans, mitotically-quiescent cardiomyocytes do not re-enter the cell cycle in sufficient numbers to proliferatively repair the heart after injury [1, 2]. This poses a significant clinical impediment for effective treatment of human heart disease, which remains the leading cause of morbidity and mortality worldwide [3]. In neonatal rodents, cardiomyocytes transition from a proliferative to hypertrophic mode of growth in the first few days after birth [4, 5]. Rodent cardiomyocytes undergo cell cycle arrest by postnatal day (P)7, and concurrently lose their capacity for proliferative regenerative repair following injury [5, 6]. The numbers of mononucleated-diploid cardiomyocytes capable of proliferating to generate new cardiomyocytes are also reduced and cardiomyocyte binucleation is initiated in the first week after birth [7]. Loss of developmental signaling and activation of cell cycle inhibitory factors, influenced by increased oxidative stress and metabolic maturation, together modulate this early neonatal cardiomyocyte cell cycle arrest in rodents [8, 9]. However, the regulatory mechanisms that coordinate cardiomyocyte cell cycle arrest with other maturational processes after birth are not fully known.

Depletion of cell cycle inhibitory genes has been pursued as a strategy to reactivate cardiomyocyte proliferation in postnatal hearts. These include Meis1, a homeobox transcription factor [10], Forkhead Box O1 and O3 transcription factors (FoxO1/O3) [11], and anti-proliferative cell cycle checkpoint genes such as p21, p27, and p57 [12]. However, in all these loss-of-function strategies, the increase in cardiomyocyte mitotic activity is limited, and cardiomyocyte terminal maturation occurs within the first few postnatal weeks [10, 11]. Similarly, maintenance of cardiomyocytes in a hypoxic environment after birth extends the period of increased proliferation and regenerative capacity from P0 to P7, but cell cycle arrest and loss of regenerative potential still occur in the subsequent weeks [9, 13]. These studies indicate that multiple functional redundancies need to be overcome to robustly extend cardiomyocyte cell cycle activity in the post-mitotic heart beyond the postnatal period. Overexpression of cell cycle activators such as ErbB2 in cardiomyocytes can induce proliferation in the long term, but these approaches lead to uncontrolled cardiomyocyte proliferation resulting in cardiomegaly or cardiomyocyte polyploidization and ultimately heart failure [14]. It is thus necessary to identify reinforcing mechanisms that contribute to

Author Manuscript Author Manuscript Author Manuscript Author Manuscript

cardiomyocyte cell cycle arrest in neonatal rodents to improve strategies for cardiomyocyte proliferative repair without cardiomegaly in adult disease.

Previously, we showed that overexpression of developmental T-box transcription factor Tbx20 promotes cardiomyocyte proliferation via direct repression of anti-proliferative genes *p21* and *Meis1*, as well as *Btg2* [15]. Btg2 belongs to a family of *Btg* (B-cell translocation gene)/Tob anti-proliferative genes with unknown functions in the heart. In immune and cancer cell lineages, Btg2 and closely-related Btg1 (Btg1/2) were identified as transcriptional co-regulators of the anti-proliferative Btg/Tob family, sharing high structural similarity and potential functional redundancy [16–18]. Btg1/2 are multifunctional proteins in the context of development and cancer, with reported roles in regulation of cell proliferation, differentiation, and apoptosis [19–24]. Btg1/2 are also involved in DNA damage, oxidative and ER cell stress responses, and in regulatory pathways of transcription factors such as FoxO3, ATF4 and NFkB [16]. However, the *in vivo* roles of Btg1/2 in the neonatal heart have not been reported.

In this study, mice with constitutive Btg1/2 deletion or with early neonatal knockdown of Btg1/2 by AAV9-shRNA injections were assessed for cardiomyocyte mitotic activity and maturation in the weeks after birth. Further, neonatal rat cardiomyocyte cultures with siRNA-mediated Btg1/2 knockdown were analyzed for cardiomyocyte proliferation and maturation, as well as transcriptomic changes by RNAseq. Together, these *in vivo* and *in vitro* studies support a novel role for Btg1/2 in mammalian cardiomyocyte cell cycle control and response to oxidative stress after birth.

## 2. RESULTS

### 2.1 Btg1 and Btg2 are expressed in neonatal mouse hearts

Cardiomyocyte cell cycle arrest is initiated in the first few days after birth in mice [4]. During this early postnatal period, cell cycle inhibitory factors are induced while cardiomyocyte proliferative factors are repressed [8]. To assess expression of Btg1 and Btg2 (Btg1/2) in early and late postnatal mouse ventricles, C57BL/6 wildtype mouse hearts were collected at postnatal day (P)0, P7, P15, and P30. By immunostaining of paraffin sections of wildtype mouse hearts, both Btg1 and Btg2 antibodies are broadly expressed in cardiomyocytes and other cell types of the postnatal heart (Figure 1), compared to Btg1/2-null mouse hearts used as negative staining controls (Figure S1A). This broad expression of Btg1/2 has been described previously in non-cardiac tissues and cell lineages [25]. The non-cell specific expression pattern of Btg1/2 is also observed by RNAscope *in situ* hybridization in wildtype mice, where punctate *Btg1* and *Btg2* RNA expression was detected in *Trop I* (*Troponin I*)-labeled cardiomyocytes, as well as *Col1a1* (*Collagen Type I Alpha 1*)-labeled fibroblasts (Figure S1B). To further understand the expression pattern of Btg1/2 in various cardiac cell types, we analyzed published single-cell RNA sequencing (scRNAseq) data from developing embryonic day (E)10.5 to P9 C57BL/6 hearts, described by Feng, Bais, *et al.* [26]. Processed scRNAseq expression data deposited to UCSC cell browser [26, 27] were utilized to generate Uniform Manifold Approximation and Projection (UMAP) visualization plots for gene expression (Figure S1C). Expression of *Btg1* and *Btg2* were compared to cardiac cell-specific markers such as *Nkx2–5* (cardiomyocytes), *Tcf21*

Author Manuscript Author Manuscript Author Manuscript Author Manuscript

(fibroblasts), and *Pecam1* (endothelial cells), as well as Tbx20-target *Meis1* [15]. The data show both *Btg1* and *Btg2* are expressed in most cardiac cell types, though *Btg1* is seen at higher levels compared to *Btg2*. Further, *Btg1/2* levels in developing C57BL/6 mouse hearts are comparable to *Meis1* (Figure S1C i–iii), a well-known regulator of postnatal cardiomyocyte cell cycle arrest [10]. Together, these data indicate that Btg1/2 are broadly expressed in developing mouse heart tissues.

Btg1 expression in the left ventricle in the first postnatal month is highest at P0–P7 (Figure 1A, B) coincident with onset of cardiomyocyte cell cycle arrest, and expression is decreased by P15-P30 (Figure 1A, green stain). By mRNA quantification of *Btg1* by RT-qPCR, higher gene expression of Btg1 is observed in early neonatal hearts, followed by downregulation at P15-P30 (Figure 1C). Similarly, Btg2 expression by immunostaining is also highest at P0 in postnatal mouse left ventricles, with lower expression at P7, which is further decreased by P15-P30 (Figure 1D, E). Interestingly, mRNA quantification by RT-qPCR shows that *Btg2* gene expression is maintained in the postnatal mouse heart, with no significant change from P0–P30 (Figure 1F), incongruent with its protein expression by immunostaining. Together, these data indicate that Btg1/2 expression after birth is highest in the early neonatal period, similar to other cardiac cell cycle inhibitors and concurrent with onset of cardiomyocyte cell cycle arrest.

### 2.2 Cardiomyocyte mitotic activity is increased at P7 in Btg1/2 constitutive double knockout mice

To assess whether Btg1/2 has a regulatory role in cardiomyocyte cell cycle activity *in vivo*, postnatal cardiac development was examined in previously-described constitutive double knockout mice for Btg1 and Btg2 (Btg1/2 DKO), raised on a C57BL/6 background [17]. Hearts were collected at P7 and P30 (Figure 2A), to identify whether systemic Btg1/2 deletion affected cardiomyocyte mitotic activity and hypertrophy during neonatal cell cycle arrest (P7) and in mature quiescent hearts (P30). *Btg1* and *Btg2* mRNA quantification by RT-qPCR confirmed loss of Btg1/2 expression in postnatal mouse ventricles (Figure 2B). Systemic genomic deletion of Btg1/2 did not affect normal cardiac development, with no significant change in heart weight-to-body weight ratios (HW/BW) of Btg1/2 DKO mice compared to age-matched Wildtype (WT) controls at P7 or P30 (Figure 2C). Further, there was no change in cardiomyocyte cell size or morphology of Btg1/2 DKO mouse hearts compared to WT, as indicated by cardiomyocyte (CM) cross-sectional area measurements at P7 and P30. Cross-sectional area was assessed by manual tracing of sarcomeric α-actinin-stained cardiomyocytes with wheat germ agglutinin (WGA) co-staining to define cell boundaries (Figure 2D, E). Cardiomyocyte cross-sectional area was also not significantly increased in aged (12–14 postnatal months) Btg1/2 DKO mice compared to age-matched WT controls (Figure S2), indicating there is no apparent late-stage pathological remodeling of the heart upon systemic Btg1/2 loss from early embryonic development.

Cardiomyocyte mitotic activity was assessed in Btg1/2 DKO mouse left ventricles and WT controls, utilizing Phosphohistone H3 (pHH3) to stain mitotically-active nuclei, together with Desmin or α-actinin co-staining of cardiomyocyte sarcomeres (Figure 2F, G). Increased overall expression of pHH3 was observed in the left ventricular tissues of Btg1/2 DKO mice

Author Manuscript Author Manuscript Author Manuscript Author Manuscript

at P7 compared to WT (Figure 2F). To accurately assign pHH3+ nuclei to cardiomyocyte (CM) mitotic activity in paraffin sections, Z-stack images of Btg1/2 DKO and WT mouse left ventricles, stained with pHH3 and sarcomeric α-actinin, were obtained (Figure 2G). Manual counts of pHH3-positive cardiomyocyte nuclei revealed significantly increased cardiomyocyte mitotic activity at P7 in Btg1/2 DKO mice compared to WT (Figure 2H). However, there is no difference in cardiomyocyte mitotic activity at P30 between Btg1/2 DKO and WT mice. Further, non-cardiomyocyte (NonCM) mitotic activity, obtained by manual counts of pHH3-positive nuclei in WGA-defined cells negative for sarcomeric α-actinin, was also not significantly different between Btg1/2 DKO and WT mice at P7 or P30 (Figure 2I). Together, these results indicate that systemic Btg1/2 deletion increases cardiomyocyte-specific mitotic activity in the heart at P7. However, constitutive Btg1/2 loss does not extend cardiomyocyte cell cycle activity beyond the neonatal period, and cell cycle activity is virtually undetectable by P30 in both Btg1/2 DKO and WT mouse hearts.

### 2.3 Neonatal AAV9-mediated double knockdown of Btg1/2 in mice promotes cardiomyocyte cell cycle activity at P7

To assess effect of temporally-restricted depletion of Btg1/2 in early neonatal mouse hearts, gene silencing by short-hairpin (sh)RNA delivery via adeno-associated virus serotype 9 (AAV9) was utilized. Commercially-available AAV9-shBtg1 and AAV9-shBtg2 expression vectors were obtained (Vector Biolabs, USA), for expression of shRNA from a ubiquitously-expressed U6 promoter linked to reporter genes for either green fluorescent protein (GFP) for shBtg1 or red fluorescent protein (mCherry) for shBtg2. Btg1/2 double knockdown (Btg1/2 DKD) cohorts were generated by intrathoracic injections of AAV9-shBtg1 and AAV9-shBtg2 together in newborn C57BL/6 mice at P0, with littermate AAV9-shScramble injected pups serving as controls (Figure 3A).

Hearts were collected at 7- and 14-days post-injection (7dpi and 14dpi respectively). Heart weight-to-body weight (HW/BW) ratios of Btg1/2 DKD mice were not significantly different from Scramble controls at 7dpi (Figure 3B). However, by 14dpi, HW/BW were significantly higher in Btg1/2 DKD mice compared to littermate Scramble controls (Figure 3B). Masson's Trichrome staining of whole heart paraffin sections also showed that Btg1/2 DKD mice exhibit apparent left ventricular chamber dilation and abnormal cardiac morphology at 14dpi, compared to Scramble (Figure 3C). Quantification of *Btg1* and *Btg2* gene expression by RT-qPCR confirmed ~50% decrease in Btg1/2 expression by 7dpi in whole ventricular mRNA of Btg1/2 DKD mice, compared to Scramble (Figure 3D). Note that some of the residual Btg1/2 expression measured could be in non-cardiomyocytes since AAV9 transduction is preferential in cardiomyocytes of the heart. Immunostaining for GFP alone (Scramble) or GFP and mCherry co-staining (Btg1/2) also showed high viral transduction in all AAV9-injected groups by 7dpi, which was maintained at 14dpi (Figure 3E).

Cardiomyocyte (CM) cross-sectional area was assessed in Btg1/2 DKD and Scramble tissues co-stained with α-actinin and WGA. No significant change in cardiomyocyte cross-sectional area was observed at 7dpi in AAV9-mediated Btg1/2 DKD mice compared to Scramble (Figure 3F, G). However, by 14dpi, cardiomyocyte cross-sectional area in Btg1/2

Author Manuscript Author Manuscript Author Manuscript Author Manuscript

DKD is significantly increased compared to littermate Scramble controls. This is different from constitutive Btg1/2-deleted mice where cross-sectional area does not significantly differ between Btg1/2 DKO and WT groups, even more than a year after birth (Figure 2, S2). These results suggest compensatory adaptations may be occurring with constitutive Btg1/2 deletion from embryonic stages, which are not present during rapid shRNA-mediated depletion of Btg1/2 in neonatal myocardium.

To determine if cell cycling was affected with loss of Btg1/2 after birth, cardiomyocyte mitotic activity was assessed in AAV9-injected mice by EdU (5-ethynyl-2'-deoxyuridine) incorporation *in vivo* (Figure 3H, I). EdU-positive cardiomyocyte nuclei were identified (Figure 3H), and cardiomyocyte mitotic activity was measured at 7dpi and 14dpi in Btg1/2 DKD mice compared to littermate Scramble controls (Figure 3I). At 7dpi, EdU+ cardiomyocyte nuclei were significantly increased in Btg1/2DKD hearts. However, by 14dpi, cardiomyocyte mitotic activity was similar in Btg1/2 DKD and Scramble AAV9-injected mice. These data indicate that depletion of Btg1/2 in newborn mice transiently increases cardiomyocyte mitotic activity in the first postnatal week. However, cell cycle arrest still occurs by two postnatal weeks in Btg1/2-depleted mouse cardiomyocytes.

Together with the results from constitutive Btg1/2-deleted mice (Figure 2), these data indicate that depletion of both Btg1 and Btg2 is sufficient to promote additional cardiomyocyte cell cycle activity at P7 *in vivo*. However, subsequent cell cycle arrest still occurs, which is apparent at P14.

### 2.4 Neonatal AAV9-mediated single knockdowns of Btg1 and Btg2 in mice suggest potentially greater role for Btg1 in cardiomyocyte cell cycle activity

To assess individual roles of Btg1 and Btg2 in regulating cardiomyocyte cell cycle activity in postnatal mice, commercially-available AAV9-shBtg1 and AAV9-shBtg2 were utilized individually as described above (Figure 3). Btg1 single knockdown (Btg1 SKD) and Btg2 single knockdown (Btg2 SKD) cohorts were obtained by intrathoracic injections of AAV9-shBtg1 or AAV9-shBtg2 respectively at P0 in C57BL/6 mice, with age-matched/littermate AAV9-shScramble injected mice serving as controls (Figure S3A). Hearts were harvested at 7- and 14-days post-injection (7dpi and 14dpi respectively). Immunostaining for GFP or mCherry visualized high AAV9 transduction in Btg1 SKD and Btg2 SKD left ventricular tissues respectively (Figure S3B). Similar to AAV9-mediated Btg1/2 DKD mice, at 7dpi heart weight-to-body weight ratios (HW/BW) were not different between Btg1 SKD and Btg2 SKD vs. Scramble mice (Figure S3C). However, by 14dpi, HW/BW were significantly increased in both Btg1/2 SKDs compared to Scramble (Figure S3D). When cardiomyocyte cross-sectional area was measured by co-staining for α-actinin and WGA in paraffin sections, cell area was increased in Btg2 SKD at 7dpi compared to littermate Scramble controls (Figure S3E, F). However, by 14dpi, Btg1 SKD cardiomyocytes exhibited larger cross-sectional size compared to Scramble (Figure S3E, G). Further, cardiomyocyte (CM) mitotic activity was estimated by EdU incorporation as described previously (Figure 3). EdU incorporation was in Btg1 and Btg2 SKD mouse tissues at 7dpi and 14dpi (Figure S3H). Interestingly, cardiomyocyte mitotic activity at 7dpi was significantly increased only in Btg1 SKD mice compared to Scramble, but not in Btg2 SKD mice (Figure S3H, I).

Author Manuscript Author Manuscript Author Manuscript Author Manuscript

By 14dpi, cardiomyocyte mitotic activity in Btg1/2 SKD and Scramble mice were at a similarly low level (Figure S3H, J). Together, these data suggest Btg1 and Btg2 may be differentially-regulated in cardiomyocyte cell cycle activity and maturation in early postnatal mice. Higher cardiomyocyte mitotic activity in Btg1 SKD alone compared to Btg2 SKD at 7dpi (Figure S3H–J) suggests Btg1 may play a greater role compared to Btg2 in regulating postnatal cardiomyocyte mitotic activity *in vivo*.

### 2.5 Depletion of Btg1/2 via siRNA promotes cardiomyocyte proliferative activity *in vitro*

To assess cardiomyocyte-specific effects of Btg1/2 depletion, cultured neonatal rat ventricular myocytes (NRVM) were utilized. Primary cardiomyocytes isolated from newborn rat ventricles were cultured for two days and subsequently incubated in Btg1/2 siRNA cocktails, with Scramble siRNA treatment as control (Figure 4A). Btg1/2 double knockdown (Btg1/2 DKD) and single knockdown (Btg1 SKD, Btg2 SKD) groups were treated in independent culture wells. RT-qPCR quantification of *Btg1* and *Btg2* mRNA expression at 48 hours post-transfection showed ~70–80% knockdown efficiency for Btg1/2 in all single- and double- knockdown cultures, compared to Scramble-treated controls (Figure 4B). Cardiomyocyte mitotic activity was assessed by EdU treatment of Btg1/2-depleted NRVMs for 6 hours and followed by staining to detect nuclear EdU incorporation (Figure 4C i-iv). Cardiomyocytes vs. non-cardiomyocytes were identified by co-staining for sarcomeric Troponin I and Vimentin respectively. Cardiomyocyte (CM) mitotic activity was measured in all Btg1/2 knockdown cohorts by manual counts for EdU-positive nuclei, compared to Scramble-treated controls (Figure 4D). In Btg1/2 DKD cultures, cardiomyocyte mitotic activity is significantly increased compared to Scramble-treated controls and falls between the levels measured in Btg1 SKD and Btg2 SKD groups, similar to AAV9-mediated Btg1/2 SKDs (Figure S3). These data further support Btg1 as a preferential regulator of cardiomyocyte cell cycling in neonatal rodent hearts, compared to Btg2.

To assess whether increased cardiomyocyte mitotic activity upon Btg1/2 depletion is due to an increase in binucleated cardiomyocytes, nucleation counts were performed. The number of mononucleated (1 nucleus) and binucleated (2 nuclei) cardiomyocytes per area were manually counted in siRNA-treated NRVMs (Figure 4C v–vi). No significant increase in cardiomyocyte binucleation was observed in Btg1/2-depleted groups compared to Scramble (Figure 4E). However, the percentage of mononucleated cardiomyocytes was also unchanged across Btg1/2-depleted and Scramble NRVM groups. To assess whether ploidy is increased in Btg1/2-depleted groups, nuclear DAPI fluorescence intensities of Troponin I (cardiomyocyte, CM) or Vimentin (non-cardiomyocyte, NonCM) labeled cells were measured (Figure 4C, F). Cardiomyocyte nuclear intensities were normalized to diploid non-cardiomyocyte nuclear intensities per area, and thresholds for diploid (2c) and polyploid (2c<) nuclear DNA content were determined as described previously [7, 28]. There is no significant increase in cardiomyocyte nuclear polyploidy in Btg1/2-depleted groups compared to Scramble control (Figure 4F). Interestingly, increased proportion of diploid nuclei was observed in Btg1 SKD relative to Scramble, reinforcing the potential preferential role for Btg1 in cardiomyocyte proliferative activity as described above (Figure S3). Together, these data show that increased cardiomyocyte mitotic activity upon Btg1/2-depletion is due to proliferation, not endoreplication.

Author Manuscript Author Manuscript Author Manuscript Author Manuscript

Further, the proportion of cardiomyocytes (CM) vs. non-cardiomyocytes (NonCM) per area was not significantly different between Btg1/2-depleted and Scramble NRVM groups (Figure S4A). Also, non-cardiomyocyte mitotic activity, assessed by Vimentin co-staining with EdU, is not significantly different in Btg1/2-depleted NRVMs compared to Scramble (Figure S4B, C). These data show that induction of proliferative activity occurs primarily in cardiomyocytes upon siRNA-mediated knockdown of Btg1/2 *in vitro*.

### 2.6 Transcriptomic analysis of Btg1/2-depleted cardiomyocytes by RNAseq

Simultaneous loss of both Btg1 and Btg2, *in vivo* or *in vitro*, increases cardiomyocyte mitotic activity in neonatal rodents (Figure 2–4). To identify global changes in mRNA expression due to Btg1/2 depletion, RNAseq of siRNA-transfected NVRMs was performed. Total RNA was isolated from Btg1/2 DKD, Btg1 SKD, Btg2 SKD, and Scramble (Scr) NRVM treatment groups at 48 hours post-transfection (Figure 5A). Principal component analysis (PCA) plot shows segregation of biological replicates for all Btg1/2-depleted and Scramble-treated cohorts (Figure 5B). Interestingly, Btg2 SKD and Scramble were clustered closer together with higher variation compared to Btg1 SKD and Btg1/2 DKD groups. This indicates that Btg1 SKD and Btg1/2 DKD treatment cohorts exhibit greater significant differences in transcriptomic gene expression, compared to Scramble control. By Venn intersection analysis between the three comparison groups (Btg1 SKD vs. Scr, Btg2 SKD vs. Scr, and Btg1/2 DKD vs. Scr), overlap of the 786 total significantly differentially expressed genes was visualized (Figure 5C, S5). High overlap was observed between significantly differentially expressed genes of Btg1 SKD vs. Scr and Btg1/2 DKD vs. Scr comparison groups. These data are consistent with observations of Btg1 knockdown leading to greatest increase in cardiomyocyte cell cycle activity among Btg1/2-depleted groups (Figure 4, S3).

Heatmap analysis of the expression profiles of 786 total significantly differentially expressed genes shows high transcriptomic similarity in biological replicates within each siRNA treatment cohort (Figure 5D, Supplemental Table 3). As expected, Btg1 and Btg2 were among the most significantly decreased genes in the corresponding siRNA-treated groups (Supplemental Table 3). Gene ontology (GO) enrichment analysis was performed for all Btg1/2 knockdown vs. Scramble comparison groups to obtain significant Biological Process GO terms (GO-BP), using DAVID online bioinformatics analysis tool (Supplemental Table 4) [29]. Selected top GO-BP terms are provided for major known Btg1/2 regulatory processes which are also significantly altered in Btg1/2-depleted NRVMs (Figure 5E–G, Supplemental Table 4). GO-BP terms for positive regulation of cell proliferation and growth were significant in all Btg1/2 knockdown groups, confirming increased cardiomyocyte mitotic activity observed in Btg1/2-depleted mice and NRVMs by pHH3 and EdU staining (Figure 2–4, S3). However, other significant GO-BP terms in Btg1/2-depleted NRVMs such as increased angiogenic signaling were not observed *in vivo*, as vascular capillary density was unchanged in Btg1/2-depleted mouse left ventricles compared to Scramble at P7 and P14 (Figure S6). Notably, hypoxia response signaling and positive regulation of gene expression were among the top significant GO-BP terms with loss of Btg1 and/or Btg2. Modulation of oxidative stress response and changes to global transcriptional activity are known mechanisms of Btg1/2 loss in proliferation control of various cancers and non-cardiac cell lineages [16]. A critical role has also been described for oxidative metabolism

Author Manuscript Author Manuscript Author Manuscript Author Manuscript

and hypoxia response in cardiomyocyte proliferation and heart regeneration [9, 13], which could be a mechanism for Btg1/2 in the postnatal heart. Together, our RNAseq data support dynamic and pleiotropic roles for Btg1/2 in regulating cell cycle activity and oxidative stress responses in neonatal cardiomyocytes.

## 3. DISCUSSION

Here, we demonstrate for the first time that Btg1 and Btg2 regulate cardiomyocyte cell cycle activity in the early neonatal period in rodents, utilizing both *in vivo* and *in vitro* model systems. In the first few days after birth in rodents, cardiomyocyte mitotic arrest occurs, alongside a switch to hypertrophic growth and rapid binucleation [4]. At the same time, oxidative stress and DNA damage response contributes to cardiomyocyte maturation, including cell cycle arrest and loss of the capacity for innate cardiac regeneration [6, 9]. Intersecting and reinforcing cardiomyocyte cell cycle inhibitory gene programs are initiated in the late fetal to early neonatal stages and contribute to mitotic arrest and terminal maturation in rodent hearts. Our results show that Btg1/2 are among these factors that contribute to postnatal cardiomyocyte cell cycle arrest.

Loss-of-function studies with cell cycle inhibitory factors prolong cardiomyocyte cell cycle, but typically only for a few additional rounds of proliferation. For example, cardiomyocyte-specific loss of FoxO1/O3 from late fetal stages in mice leads to a transient increase in cardiomyocyte mitotic activity at P1 and P3, but cell cycle withdrawal occurs by P7 and beyond [11]. Likewise, systemic Meis1 deletion extends cardiomyocyte cell cycle activity up to P14, but mitotic arrest occurs a few weeks later [10]. Here, we describe a similar transient increase in cardiomyocyte mitotic activity *in vivo* at P7, upon constitutive loss of Btg1/2 beginning in embryonic development and also with AAV9-mediated Btg1/2-depletion specifically in newborn hearts. Thus, Btg1/2 likely function in tandem with other cardiomyocyte cell cycle inhibitors in neonatal cell cycle regulation in the heart. Also, cardiomyocyte cell cycle withdrawal by P14-P30 suggests compensatory mechanisms by other cell cycle inhibitors may be occurring in Btg1/2-depleted mouse hearts. It is not known whether Btg1/2 depletion is sufficient to reactivate cardiomyocyte proliferative activity in adult mouse hearts or promote cardiac regenerative repair after injury.

Forced expression of cardiomyocyte proliferative factors can result in uncontrolled cardiac hyperplasia and cardiomegaly, undesirable for therapeutic translation [14, 30]. Similarly, cardiomyocyte hypertrophy was observed at P14 with AAV9-mediated Btg1/2 knockdown beginning at P0, consistent with a previous report that Btg2 is a negative regulator of cardiomyocyte hypertrophy [31]. The compensatory mechanisms that balance multiple contributing factors in cardiomyocyte mitotic arrest with pathologic proliferation, hypertrophy, and cardiomegaly in adult mammalian hearts is not well-understood. Previously, we showed that Tbx20 overexpression promotes cardiomyocyte proliferative activity via activation of cardiac developmental signaling pathways including Hippo/Yap and BMP/Smad [15]. During development, Btg2 regulates vertebral patterning in embryonic mice by modulating BMP/Smad signaling [32]. Another mechanism of Tbx20 overexpression is repression of cell cycle inhibitory factors p21, Meis1, and Btg2. The homeobox transcription factor Meis1, together with its cofactor Hoxb13, has an anti-

Author Manuscript Author Manuscript Author Manuscript Author Manuscript

proliferative role in neonatal cardiomyocyte mitotic arrest [10, 33]. Similarly, Btg1/2 interact with Homeobox proteins, such as HoxB9, in mediating their antiproliferative function in epithelial cells [34]. However, how Btg1/2 intersect with these established cell cycle regulatory mechanisms in postnatal cardiomyocyte cell cycle arrest is unknown.

RNAseq analysis of transcriptomic changes revealed significant changes in cell proliferation and hypoxia response pathways in Btg1/2-depleted NRVMs compared to control group. Among the significantly differentially expressed genes regulating cell proliferation are *MYCN*, previously identified as a Btg2 target gene [31], and also ErbB4, which is implicated in neonatal cardiomyocyte cell cycle arrest [14]. Moreover, Btg1/2 are downstream effectors in p53-dependent and -independent DNA damage response pathways [35, 36], as well as in oxidative stress regulation and maintenance of cellular homeostasis in multiple cell types [24]. Changes in the hypoxia response pathway genes with Btg1/2 deficiency could be related to reports that cardiomyocyte cell cycling and regenerative potential are prolonged after birth under hypoxic conditions [9, 13]. In these studies, the increase in cardiac DNA damage due to oxidative stress and normoxic conditions upon birth was identified as an important regulator of neonatal cardiomyocyte cell cycle arrest [9]. Thus, gene expression changes upon Btg1/2 depletion in neonatal cardiomyocytes indicates a coordinating role for these genes alongside oxidative stress signaling in inducing cell cycle arrest soon after birth in mammals.

## 4. CONCLUSIONS

In this study, we report Btg1/2 are novel regulators of neonatal cardiomyocyte cell cycle arrest, potentially via cell proliferative and oxidative stress signaling. Loss of Btg1/2 leads to increased cardiomyocyte cell cycle activity at P7 followed by cell cycle arrest at P14, suggesting that multiple compensatory mechanisms co-ordinate in regulation of neonatal cardiomyocyte cell cycle arrest. Considering the complexity of neonatal cardiac maturation, understanding the interplay between Btg1/2 and other cardiomyocyte cell cycle regulators is necessary if these mechanisms are to be used for cardiac proliferative repair in disease.

## 5. METHODS

Details on all antibodies and reagents, including dilutions, working concentrations, and manufacturer catalog information, are provided in Supplemental Table 1. Primer sequences used for RT-qPCR are listed in Supplemental Table 2. RNAseq analyses are provided as Excel spreadsheets in Supplemental Tables 3 and 4.

### 5.1 Mice

All experiments with animals were performed conforming to NIH Guidelines on Care and Use of Laboratory Animals. All protocols involving animals were approved by the Cincinnati Children’s Hospital Institutional Animal Care and Use Committee (IACUC). Btg1/2 deleted mice on a C57BL/6 background [17] were acquired from Frank N. van Leeuwen (Princess Máxima Center for Pediatric Oncology, Netherlands) and Blanca Scheijen (Radboud University Medical Center, Netherlands) and used to generate neonatal Btg1/2 DKO mice in-house at the CCHMC vivarium (Cincinnati, OH, USA). Polymerase

Author Manuscript Author Manuscript Author Manuscript Author Manuscript

Chain Reaction (PCR) genotyping of Btg1/2 DKO mice was performed on DNA isolated from ear or tail clips of mice, as described previously [17]. Wildtype C57BL/6 mice were bred in-house, with founder animals originally sourced from Jackson Labs (Bar Harbor, ME, USA). Male and female mice were included in all studies, and littermate animals were used whenever possible.

### 5.2 Cardiac tissue harvest

Mouse body weights (in g) were obtained prior to euthanasia. After euthanasia with Isoflurane followed by cervical dislocation, whole hearts were harvested, exsanguinated, and weighed (in g). Freshly-harvested hearts were washed in 1X phosphate buffered saline (PBS) and placed in 4% paraformaldehyde (PFA) for histology studies or flash-frozen in liquid nitrogen for mRNA isolation. PFA-fixed hearts were subsequently dehydrated and embedded in paraffin wax for microtome sectioning. Heart weight-to-body weight ratios were calculated with Microsoft Excel.

### 5.3 AAV9-shRNA injections in neonatal mice

Wildtype C57BL/6 mice were bred in-house by timed matings, the day of birth noted as P0. Intrathoracic injections with sterile 28-gauge needle syringes were performed for AAV9-shRNA delivery in newborn littermate pups (P0) within 8 hours of birth. Commercially-available AAV9-GFP-shBtg1, AAV9-mCherry-shBtg2, and AAV9-GFP-shScramble, packaged under a U6 promoter, were utilized (Vector Biolabs, USA; catalog numbers are provided in supplement). A total of 20uL was injected per newborn mouse, with $7.5\times10^{10}$ genome count concentration of AAV9-shRNA diluted in sterile 0.9% Sodium Chloride solution.

### 5.4 Neonatal rat cardiomyocyte isolation and culture

Pregnant female Sprague-Dawley rats were obtained from Envigo (Indianapolis, IN, USA) for harvest of newborn rat hearts. Primary neonatal rat cardiomyocytes were isolated from hearts of newborn rats as described previously [37]. Following pre-plating of fibroblasts, cardiomyocyte-enriched medium was plated. About 1–3 million cells were plated on 6-well plates for mRNA isolation or 2-well chamber slides for immunofluorescence studies. Cells were incubated at 37°C in 1X Medium-199 with Earle’s salts, L-glutamine, 15% bovine growth serum and 2X penicillin/streptomycin.

### 5.5 siRNA transfections in neonatal rat cardiomyocytes

Following ~40 hours of growth *in vitro*, neonatal rat cardiomyocytes in independent culture wells were incubated in siRNA transfection cocktail for 48 hours at 37°C. Transfection cocktails were freshly prepared in Opti-MEM media with Lipofectamine 3000 transfection agent and siRNA probes. Commercially-available rat *siBtg1* and *siBtg2* and *siScramble* (Negative) control probes (Thermo Fisher Scientific, USA; catalog numbers are provided in supplement) were utilized for single- and double-knockdowns, as described previously [15]. Transfection cocktails were prepared as follows for 20nM total siRNA concentration per culture well: 10nM *siScramble* with 10nM *siBtg1* for Btg1SKD, 10nM *siScramble* with 10nM *siBtg2* for Btg2SKD, 10nM of both *siBtg1* and *siBtg2* for Btg1/2 DKD, or

Author Manuscript Author Manuscript Author Manuscript Author Manuscript

20nM *siScramble* alone for control. At 48 hours post-transfection, cells were washed in warm Dulbecco's sterile PBS, then fixed with 4% PFA for immunostaining or flash-frozen in liquid nitrogen for mRNA isolation. Cells were utilized from at least two independent neonatal cardiomyocyte isolations and culture preparations for each experiment.

### 5.6 mRNA analysis by RT-qPCR

RNA was extracted using NucleoSpin RNA Isolation Kit (Macherey-Nagel, Germany), from frozen mouse ventricular tissue or cultured cardiomyocytes. cDNA synthesis was performed using Superscript III First Strand kit (Thermo Fisher Scientific, USA) according to manufacturer's protocol. RT-qPCR was performed using SYBR Green. Gene-specific primer sets designed with NCBI PrimerBlast were ordered from IDT DNA Technologies (Coralville, IA, USA), and then validated by Sanger sequencing (Supplemental Table 2). Relative gene expression was calculated by comparative *ΔΔCt* method [38], with *18s*, *28s*, or *Gapdh* used for normalization. Normalized average expression of control groups in each analysis was set to 1.0, to calculate relative fold change in treatment groups.

### 5.7 Histochemical and fluorescence staining

Information on all antibodies and reagents, including catalog numbers and dilutions, are provided in Supplemental Table 1.

**5.7.1 Masson's Trichrome staining:** Paraffin sections were dewaxed and rehydrated by immersion in xylene and graded concentrations of ethanol respectively, as described previously [15]. Masson's Trichrome 2000 kit was used according to manufacturer's protocol and slides were coverslipped with Cytoseal 60 mounting medium. Brightfield images were captured in Olympus BX51 microscope equipped with Nikon DS-Ri1 (Tokyo, Japan).

**5.7.2 Lectin-DAB staining:** Paraffin sections were dewaxed and rehydrated, followed by antigen retrieval with 1X citrate buffer in pressure cooker at high pressure. Blocking was performed with 0.3% hydrogen peroxide and 6% goat serum for 30 minutes, followed by overnight incubation at 4°C with biotinylated lectin. Following manufacturer protocols, Avidin-Biotin Complexing kit and 3,3'-diaminobenzidine (DAB) metal concentrate in stable peroxidase were used to detect staining.

**5.7.3 Immunostaining:** Paraffin sections were baked at 60°C for 1 hour prior to dewaxing and rehydration steps. Antigen retrieval was performed with 1X citrate buffer in pressure cooker at high pressure. For PFA-fixed cultured rat cardiomyocytes in 2-chamber slides, these above steps were not performed. 1X PBS or TBS was used for all wash steps. Blocking was performed with 1X Fish skin gelatin blocking buffer for 1–2 hours at room temperature. Primary antibodies (dilutions in Supplemental Table 1) were incubated overnight at 4°C. Donkey IgG secondary antibodies were incubated for 1 hour at room temperature. Nuclei were visualized by immersion in DAPI solution in 1X PBS or TBS for 15 minutes. Vectashield Hardset mounting medium was used for coverslipping. Confocal images were obtained using Nikon Eclipse Ti Fluorescence microscope with NIS Elements imaging software (Tokyo, Japan).

Author Manuscript Author Manuscript Author Manuscript Author Manuscript

**5.7.4 RNAscope in situ hybridization:** Paraffin sections were baked at 60°C for 1 hour, followed by dewaxing and rehydration steps. RNAscope™ Multiplex Fluorescent Reagent Kit and Probes (Advanced Cell Diagnostics, USA) were used following manufacturer's protocol. Slides were coverslipped with Vectashield Hardset mounting medium. Nikon Eclipse Ti Fluorescence microscope and NIS Elements software were used to obtain confocal images.

**5.7.5 Analysis:** Staining quantification, object counting, and morphometric analyses were performed using NIS Elements and Fiji (ImageJ) analysis software, in 20X or 60X images of 4–6 random cardiac regions per paraffin tissue section or fields per culture well. Cardiomyocyte mitotic indices, cross-sectional area, vascular capillary counts, and nucleation counts were estimated by manual counting of nuclei or manual tracing of cell boundaries, as described previously [28]. For determination of nuclear DNA content by DAPI staining, the method of Patterson *et al.* [7] was modified to determine thresholds for diploid (2c) and polyploid (2c<) nuclear intensities, as described previously [28].

## 5.8 EdU incorporation assay

For EdU (5-ethynyl-2'-deoxyuridine, Thermo Fisher Scientific, USA) incorporation *in vivo*, neonatal mice were given intraperitoneal injections of EdU solution in DMSO (10mM) at 5μL per gram body weight. Hearts were harvested and processed as described in Section 5.2, at 6 hours after EdU injections. For EdU incorporation *in vitro*, siRNA-treated cultured cardiomyocytes were treated with 10μM EdU in Opti-MEM media at 42 hours post-transfection. At 6 hours post-EdU treatment, cultured cardiomyocytes were processed for analysis as described in Section 5.5. EdU staining was visualized using Click iT Alexa Fluor Imaging Kit (Fisher Scientific, USA) following manufacturer's protocol.

## 5.9 Sequencing methods

**5.9.1 RNAseq analysis:** Total RNA isolated from neonatal rat cultured cardiomyocytes at 48 hours post-transfection was used for library generation and sequencing at the CCHMC Sequencing core. RNAseq reads in FASTQ format were subjected to quality control and trimming using FastQC, Trim Galore, and Cutadapt programs. Trimmed reads were then aligned to rat reference genome version rn5 using STAR program [39]. Aligned reads were stripped of duplicates using Sambamba program [40]. Read counting was done with the Rsubread package [41]. Raw counts were normalized as transcripts per million (TPM) and differential gene expression between groups was assessed with the Rpackage DESeq2 [42]. Genes with log2 fold change >= |0.58| were selected for downstream functional annotation and pathway analysis (Gene Ontology) analysis using DAVID online analysis tool [29]. An adjusted p-value cutoff of ≤0.05 was used to select significant functional annotations and pathways. Heatmap was generated using the Morpheus matrix visualization online tool (RRID:SCR_017386, Broad Institute, MA, USA). Venn intersection analysis was performed using Venny 2.1.0 and BioVenn online tools [43, 44]. Raw data files are available in the GEO database (GSE203493).

**5.9.2 Single-cell RNAseq analysis:** ScRNAseq data from E10.5 to P9 C57BL/6 mouse hearts, as analyzed and reported previously [26], was used for gene expression

Author Manuscript Author Manuscript Author Manuscript Author Manuscript

analysis. Uniform Manifold Approximation and Projection (UMAP) plots were generated with UCSC cell browser interactive online tool [27], using the processed data deposited by Feng, Bais, *et al.* at: https://mouse-dev-heart.cells.ucsc.edu (Cell Browser dataset ID: mouse-dev-heart) [26]. All gene expression analyses were performed with 'Mouse Developing Heart – C57BL/6 Wild Type Strain' dataset.

### 5.10 Statistics

Graphical visualization and statistical analyses were performed using GraphPad Prism 8 software. Unpaired non-parametric tests, such as Mann Whitney's U-test or Dunn's Kruskal-Wallis Multiple Comparisons tests were used unless noted otherwise. $p<0.05$ was deemed significant in all analyses.

## Supplementary Material

Refer to Web version on PubMed Central for supplementary material.

## ACKNOWLEDGEMENTS

We thank Dr. Kelly Grimes (Cincinnati Children's Hospital, Cincinnati, OH, USA) for critical suggestions in optimizing neonatal AAV9-mediated gene depletion mouse models, and Dr. Leah Kottyan (Cincinnati Children's Hospital, Cincinnati, OH, USA) for valuable discussions on next-generation sequencing protocols. We also thank the Division of Biomedical Informatics at Cincinnati Children's Hospital (Cincinnati, OH, USA) for technical assistance in analyzing RNAseq datasets.

#### FUNDING

This work was supported by the National Institutes of Health [R01HL135848 to KEY, T32HL125204 and F32HL159894 to SLP]; American Heart Association Predoctoral Fellowship [19PRE34380046 to NV]; and the Cincinnati Children's Research Foundation.

## REFERENCES

[1]. Bergmann O, Bhardwaj RD, Bernard S, Zdunek S, Barnabe-Heider F, Walsh S, Zupicich J, Alkass K, Buchholz BA, Druid H, Jovinge S, Frisen J, Evidence for cardiomyocyte renewal in humans, Science 324(5923) (2009) 98–102. [PubMed: 19342590]

[2]. Bergmann O, Zdunek S, Felker A, Salehpour M, Alkass K, Bernard S, Sjostrom SL, Szewczykowska M, Jackowska T, Dos Remedios C, Malm T, Andra M, Jashari R, Nyengaard JR, Possnert G, Jovinge S, Druid H, Frisen J, Dynamics of Cell Generation and Turnover in the Human Heart, Cell 161(7) (2015) 1566–75. [PubMed: 26073943]

[3]. Virani SS, Alonso A, Benjamin EJ, Bittencourt MS, Callaway CW, Carson AP, Chamberlain AM, Chang AR, Cheng S, Delling FN, Djousse L, Elkind MSV, Ferguson JF, Fornage M, Khan SS, Kissela BM, Knutson KL, Kwan TW, Lackland DT, Lewis TT, Lichtman JH, Longenecker CT, Loop MS, Lutsey PL, Martin SS, Matsushita K, Moran AE, Mussolino ME, Perak AM, Rosamond WD, Roth GA, Sampson UKA, Satou GM, Schroeder EB, Shah SH, Shay CM, Spartano NL, Stokes A, Tirschwell DL, VanWagner LB, Tsao CW, E. American Heart Association Council on, C. Prevention Statistics, S. Stroke Statistics, Heart Disease and Stroke Statistics-2020 Update: A Report From the American Heart Association, Circulation 141(9) (2020) e139–e596. [PubMed: 31992061]

[4]. Soonpaa MH, Kim KK, Pajak L, Franklin M, Field LJ, Cardiomyocyte DNA synthesis and binucleation during murine development, Am J Physiol 271(5 Pt 2) (1996) H2183–9. [PubMed: 8945939]

Author Manuscript Author Manuscript Author Manuscript Author Manuscript

[5]. Li F, Wang X, Capasso JM, Gerdes AM, Rapid transition of cardiac myocytes from hyperplasia to hypertrophy during postnatal development, J Mol Cell Cardiol 28(8) (1996) 1737–46. [PubMed: 8877783]

[6]. Porrello ER, Mahmoud AI, Simpson E, Hill JA, Richardson JA, Olson EN, Sadek HA, Transient regenerative potential of the neonatal mouse heart, Science 331(6020) (2011) 1078–80. [PubMed: 21350179]

[7]. Patterson M, Barske L, Van Handel B, Rau CD, Gan P, Sharma A, Parikh S, Denholtz M, Huang Y, Yamaguchi Y, Shen H, Allayee H, Crump JG, Force TI, Lien CL, Makita T, Lusis AJ, Kumar SR, Sucov HM, Frequency of mononuclear diploid cardiomyocytes underlies natural variation in heart regeneration, Nat Genet 49(9) (2017) 1346–1353. [PubMed: 28783163]

[8]. Padula SL, Velayutham N, Yutzey KE, Transcriptional Regulation of Postnatal Cardiomyocyte Maturation and Regeneration, Int J Mol Sci 22(6) (2021).

[9]. Puente BN, Kimura W, Muralidhar SA, Moon J, Amatruda JF, Phelps KL, Grinsfelder D, Rothermel BA, Chen R, Garcia JA, Santos CX, Thet S, Mori E, Kinter MT, Rindler PM, Zacchigna S, Mukherjee S, Chen DJ, Mahmoud AI, Giacca M, Rabinovitch PS, Aroumougame A, Shah AM, Szweda LI, Sadek HA, The oxygen-rich postnatal environment induces cardiomyocyte cell-cycle arrest through DNA damage response, Cell 157(3) (2014) 565–79. [PubMed: 24766806]

[10]. Mahmoud AI, Kocabas F, Muralidhar SA, Kimura W, Koura AS, Thet S, Porrello ER, Sadek HA, Meis1 regulates postnatal cardiomyocyte cell cycle arrest, Nature 497(7448) (2013) 249–253. [PubMed: 23594737]

[11]. Sengupta A, Kalinichenko VV, Yutzey KE, FoxO1 and FoxM1 transcription factors have antagonistic functions in neonatal cardiomyocyte cell-cycle withdrawal and IGF1 gene regulation, Circ Res 112(2) (2013) 267–77. [PubMed: 23152492]

[12]. Di Stefano V, Giacca M, Capogrossi MC, Crescenzi M, Martelli F, Knockdown of cyclin-dependent kinase inhibitors induces cardiomyocyte re-entry in the cell cycle, J Biol Chem 286(10) (2011) 8644–8654. [PubMed: 21209082]

[13]. Nakada Y, Canseco DC, Thet S, Abdisalaam S, Asaithamby A, Santos CX, Shah AM, Zhang H, Faber JE, Kinter MT, Szweda LI, Xing C, Hu Z, Deberardinis RJ, Schiattarella G, Hill JA, Oz O, Lu Z, Zhang CC, Kimura W, Sadek HA, Hypoxia induces heart regeneration in adult mice, Nature 541(7636) (2017) 222–227. [PubMed: 27798600]

[14]. D'Uva G, Aharonov A, Lauriola M, Kain D, Yahalom-Ronen Y, Carvalho S, Weisinger K, Bassat E, Rajchman D, Yifa O, Lysenko M, Konfino T, Hegesh J, Brenner O, Neeman M, Yarden Y, Leor J, Sarig R, Harvey RP, Tzahor E, ERBB2 triggers mammalian heart regeneration by promoting cardiomyocyte dedifferentiation and proliferation, Nat Cell Biol 17(5) (2015) 627–38. [PubMed: 25848746]

[15]. Xiang FL, Guo M, Yutzey KE, Overexpression of Tbx20 in Adult Cardiomyocytes Promotes Proliferation and Improves Cardiac Function After Myocardial Infarction, Circulation 133(11) (2016) 1081–92. [PubMed: 26841808]

[16]. Yuniati L, Scheijen B, van der Meer LT, van Leeuwen FN, Tumor suppressors BTG1 and BTG2: Beyond growth control, J Cell Physiol 234(5) (2019) 5379–5389. [PubMed: 30350856]

[17]. Tijchon E, van Ingen Schenau D, van Opzeeland F, Tirone F, Hoogerbrugge PM, Van Leeuwen FN, Scheijen B, Targeted Deletion of Btg1 and Btg2 Results in Homeotic Transformation of the Axial Skeleton, PLoS One 10(7) (2015) e0131481. [PubMed: 26218146]

[18]. Hwang SS, Lim J, Yu Z, Kong P, Sefik E, Xu H, Harman CCD, Kim LK, Lee GR, Li HB, Flavell RA, mRNA destabilization by BTG1 and BTG2 maintains T cell quiescence, Science 367(6483) (2020) 1255–1260. [PubMed: 32165587]

[19]. Rouault JP, Rimokh R, Tessa C, Paranhos G, Ffrench M, Duret L, Garoccio M, Germain D, Samarut J, Magaud JP, BTG1, a member of a new family of antiproliferative genes, EMBO J 11(4) (1992) 1663–70. [PubMed: 1373383]

[20]. Lim IK, Lee MS, Ryu MS, Park TJ, Fujiki H, Eguchi H, Paik WK, Induction of growth inhibition of 293 cells by downregulation of the cyclin E and cyclin-dependent kinase 4 proteins due to overexpression of TIS21, Mol Carcinog 23(1) (1998) 25–35. [PubMed: 9766435]

Author Manuscript Author Manuscript Author Manuscript Author Manuscript

[21]. Farioli-Vecchioli S, Saraulli D, Costanzi M, Leonardi L, Cina I, Micheli L, Nutini M, Longone P, Oh SP, Cestari V, Tirone F, Impaired terminal differentiation of hippocampal granule neurons and defective contextual memory in PC3/Tis21 knockout mice, PLoS One 4(12) (2009) e8339. [PubMed: 20020054]

[22]. Farioli-Vecchioli S, Micheli L, Saraulli D, Ceccarelli M, Cannas S, Scardigli R, Leonardi L, Cina I, Costanzi M, Ciotti MT, Moreira P, Rouault JP, Cestari V, Tirone F, Btg1 is Required to Maintain the Pool of Stem and Progenitor Cells of the Dentate Gyrus and Subventricular Zone, Front Neurosci 6 (2012) 124. [PubMed: 22969701]

[23]. Yuniati L, van der Meer LT, Tijchon E, van Ingen Schenau D, van Emst L, Levers M, Palit SA, Rodenbach C, Poelmans G, Hoogerbrugge PM, Shan J, Kilberg MS, Scheijen B, van Leeuwen FN, Tumor suppressor BTG1 promotes PRMT1-mediated ATF4 function in response to cellular stress, Oncotarget 7(3) (2016) 3128–43. [PubMed: 26657730]

[24]. Imran M, Lim IK, Regulation of Btg2(/TIS21/PC3) expression via reactive oxygen species-protein kinase C-NuFkappaBeta pathway under stress conditions, Cell Signal 25(12) (2013) 2400–12. [PubMed: 23876794]

[25]. Prevot D, Morel AP, Voeltzel T, Rostan MC, Rimokh R, Magaud JP, Corbo L, Relationships of the antiproliferative proteins BTG1 and BTG2 with CAF1, the human homolog of a component of the yeast CCR4 transcriptional complex: involvement in estrogen receptor alpha signaling pathway, J Biol Chem 276(13) (2001) 9640–8. [PubMed: 11136725]

[26]. Feng W, Bais A, He H, Rios C, Jiang S, Xu J, Chang C, Kostka D, Li G, Single-cell transcriptomic analysis identifies murine heart molecular features at embryonic and neonatal stages, Nat Commun 13(1) (2022) 7960. [PubMed: 36575170]

[27]. Speir ML, Bhaduri A, Markov NS, Moreno P, Nowakowski TJ, Papatheodorou I, Pollen AA, Raney BJ, Seninge L, Kent WJ, Haeussler M, UCSC Cell Browser: Visualize Your Single-Cell Data, Bioinformatics 37(23) (2021) 4578–80. [PubMed: 34244710]

[28]. Velayutham N, Alfieri CM, Agnew EJ, Riggs KW, Baker RS, Ponny SR, Zafar F, Yutzey KE, Cardiomyocyte cell cycling, maturation, and growth by multinucleation in postnatal swine, J Mol Cell Cardiol 146 (2020) 95–108. [PubMed: 32710980]

[29]. Dennis G Jr., Sherman BT, Hosack DA, Yang J, Gao W, Lane HC, Lempicki RA, DAVID: Database for Annotation, Visualization, and Integrated Discovery, Genome Biol 4(5) (2003) P3. [PubMed: 12734009]

[30]. Gabisonia K, Prosdocimo G, Aquaro GD, Carlucci L, Zentilin L, Secco I, Ali H, Braga L, Gorgodze N, Bernini F, Burchielli S, Collesi C, Zandona L, Sinagra G, Piacenti M, Zacchigna S, Bussani R, Recchia FA, Giacca M, MicroRNA therapy stimulates uncontrolled cardiac repair after myocardial infarction in pigs, Nature 569(7756) (2019) 418–422. [PubMed: 31068698]

[31]. Masumura Y, Higo S, Asano Y, Kato H, Yan Y, Ishino S, Tsukamoto O, Kioka H, Hayashi T, Shintani Y, Yamazaki S, Minamino T, Kitakaze M, Komuro I, Takashima S, Sakata Y, Btg2 is a Negative Regulator of Cardiomyocyte Hypertrophy through a Decrease in Cytosolic RNA, Sci Rep 6 (2016) 28592. [PubMed: 27346836]

[32]. Park S, Lee YJ, Lee HJ, Seki T, Hong KH, Park J, Beppu H, Lim IK, Yoon JW, Li E, Kim SJ, Oh SP, B-cell translocation gene 2 (Btg2) regulates vertebral patterning by modulating bone morphogenetic protein/smad signaling, Mol Cell Biol 24(23) (2004) 10256–62. [PubMed: 15542835]

[33]. Nguyen NUN, Canseco DC, Xiao F, Nakada Y, Li S, Lam NT, Muralidhar SA, Savla JJ, Hill JA, Le V, Zidan KA, El-Feky HW, Wang Z, Ahmed MS, Hubbi ME, Menendez-Montes I, Moon J, Ali SR, Le V, Villalobos E, Mohamed MS, Elhelaly WM, Thet S, Anene-Nzelu CG, Tan WLW, Foo RS, Meng X, Kanchwala M, Xing C, Roy J, Cyert MS, Rothermel BA, Sadek HA, A calcineurin-Hoxb13 axis regulates growth mode of mammalian cardiomyocytes, Nature 582(7811) (2020) 271–276. [PubMed: 32499640]

[34]. Prevot D, Voeltzel T, Birot AM, Morel AP, Rostan MC, Magaud JP, Corbo L, The leukemia-associated protein Btg1 and the p53-regulated protein Btg2 interact with the homeoprotein Hoxb9 and enhance its transcriptional activation, J Biol Chem 275(1) (2000) 147–53. [PubMed: 10617598]

[35]. Choi KS, Kim JY, Lim SK, Choi YW, Kim YH, Kang SY, Park TJ, Lim IK, TIS21(/BTG2/PC3) accelerates the repair of DNA double strand breaks by enhancing Mre11 methylation

Author Manuscript Author Manuscript Author Manuscript Author Manuscript

and blocking damage signal transfer to the Chk2(T68)-p53(S20) pathway, DNA Repair (Amst) 11(12) (2012) 965–75. [PubMed: 23089312]

[36]. Cortes U, Moyret-Lalle C, Falette N, Duriez C, Ghissassi FE, Barnas C, Morel AP, Hainaut P, Magaud JP, Puisieux A, BTG gene expression in the p53-dependent and -independent cellular response to DNA damage, Mol Carcinog 27(2) (2000) 57–64. [PubMed: 10657898]

[37]. Schips TG, Vanhoutte D, Vo A, Correll RN, Brody MJ, Khalil H, Karch J, Tjondrokoesoemo A, Sargent MA, Maillet M, Ross RS, Molkentin JD, Thrombospondin-3 augments injury-induced cardiomyopathy by intracellular integrin inhibition and sarcolemmal instability, Nat Commun 10(1) (2019) 76. [PubMed: 30622267]

[38]. Livak KJ, Schmittgen TD, Analysis of relative gene expression data using real-time quantitative PCR and the 2(-Delta Delta C(T)) Method, Methods 25(4) (2001) 402–8. [PubMed: 11846609]

[39]. Dobin A, Davis CA, Schlesinger F, Drenkow J, Zaleski C, Jha S, Batut P, Chaisson M, Gingeras TR, STAR: ultrafast universal RNA-seq aligner, Bioinformatics 29(1) (2013) 15–21. [PubMed: 23104886]

[40]. Tarasov A, Vilella AJ, Cuppen E, Nijman IJ, Prins P, Sambamba: fast processing of NGS alignment formats, Bioinformatics 31(12) (2015) 2032–4. [PubMed: 25697820]

[41]. Liao Y, Smyth GK, Shi W, The R package Rsubread is easier, faster, cheaper and better for alignment and quantification of RNA sequencing reads, Nucleic Acids Res 47(8) (2019) e47. [PubMed: 30783653]

[42]. Love MI, Huber W, Anders S, Moderated estimation of fold change and dispersion for RNA-seq data with DESeq2, Genome Biol 15(12) (2014) 550. [PubMed: 25516281]

[43]. Lin G, Chai J, Yuan S, Mai C, Cai L, Murphy RW, Zhou W, Luo J, VennPainter: A Tool for the Comparison and Identification of Candidate Genes Based on Venn Diagrams, PLoS One 11(4) (2016) e0154315. [PubMed: 27120465]

[44]. Hulsen T, de Vlieg J, Alkema W, BioVenn - a web application for the comparison and visualization of biological lists using area-proportional Venn diagrams, BMC Genomics 9 (2008) 488. [PubMed: 18925949]

Author Manuscript Author Manuscript Author Manuscript Author Manuscript

**Highlights:**

- *Btg1* and *Btg2* anti-proliferative genes are expressed in early neonatal hearts.
- Btg1/2 loss *in vivo* promotes cardiomyocyte mitotic activity at postnatal day 7.
- Btg1/2 loss *in vitro* increases cardiomyocyte proliferative activity.
- RNAseq implicates proliferative and oxidative stress mechanisms in role for Btg1/2.
- Btg1 and Btg2 contribute to neonatal rodent cardiomyocyte cell cycle arrest.

Author Manuscript Author Manuscript Author Manuscript Author Manuscript

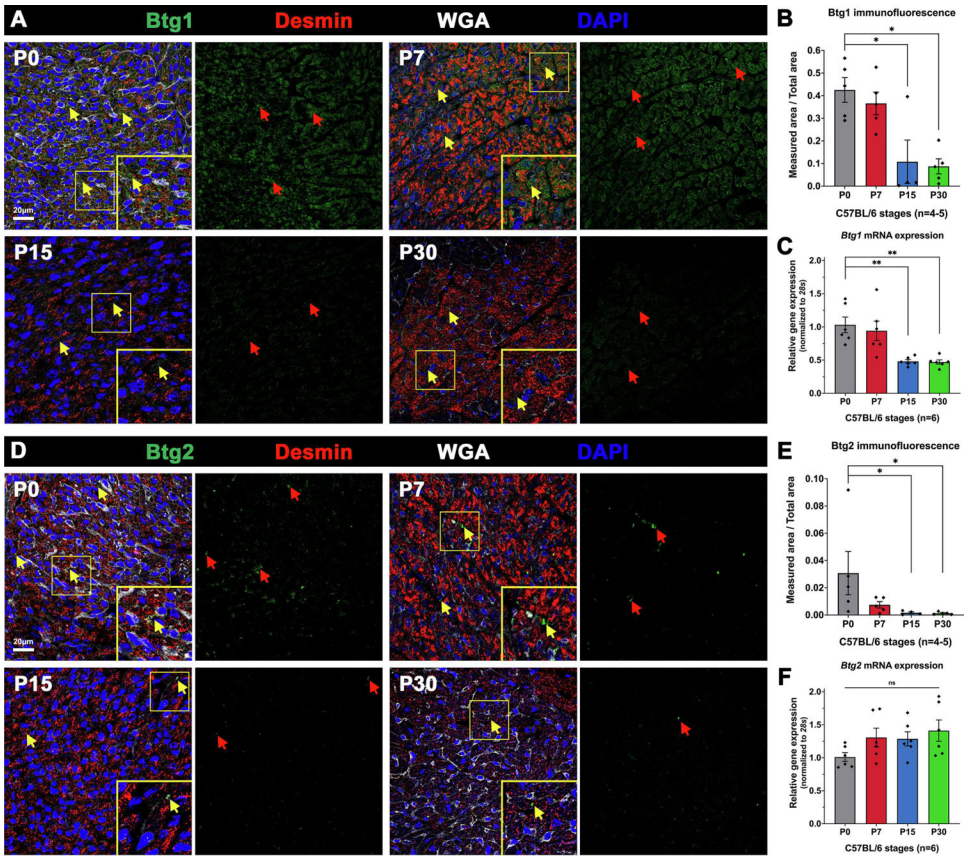


**Figure 1. Btg1 and Btg2 are expressed in early neonatal C57BL/6 mouse left ventricles.**

**(A)** Representative images of Btg1 expression detected by immunostaining at P0 (n=5), P7 (n=5), P15 (n=4), and P30 (n=5) in C57BL/6 mouse left ventricles. Yellow arrows show broad expression of Btg1 in cardiomyocytes and other cell types in the heart. Comparison of staining by red arrows indicates lower expression of Btg1 by P15 compared to P0. **(B)** Quantification of Btg1 expression by measuring green immunofluorescence per area ($0.05mm^2$), with n=4–5 mice hearts per stage and 3 tissue slices analyzed per heart. **(C)** RT-qPCR analysis of *Btg1* gene expression in neonatal mouse ventricular mRNA, with fold change relative to P0 (n=6 mice per stage). **(D)** Representative images of Btg2 expression detected by immunostaining at P0 (n=5), P7 (n=5), P15 (n=4), and P30 (n=5) in C57BL/6 mouse left ventricles. Yellow arrows show broad expression of Btg2 in cardiomyocytes and other cell types in the heart. Comparison of staining by red arrows indicates reduction in Btg2 levels by P7–P15 compared to P0. **(E)** Quantification of Btg2 expression by measuring green immunofluorescence per area ($0.05mm^2$), with n=4–5 mice per stage and 3 tissue slices analyzed per heart. **(F)** RT-qPCR analysis of *Btg2* gene expression in neonatal mouse ventricular mRNA, with fold change relative to P0 (n=6 mice per stage). Data are mean ± SEM, with *p<0.05, **p<0.01 determined with respect to P0 by Dunn's Kruskal-Wallis Multiple Comparisons Tests in P0–P30 C57BL/6 wildtype mice.

Author Manuscript Author Manuscript Author Manuscript Author Manuscript

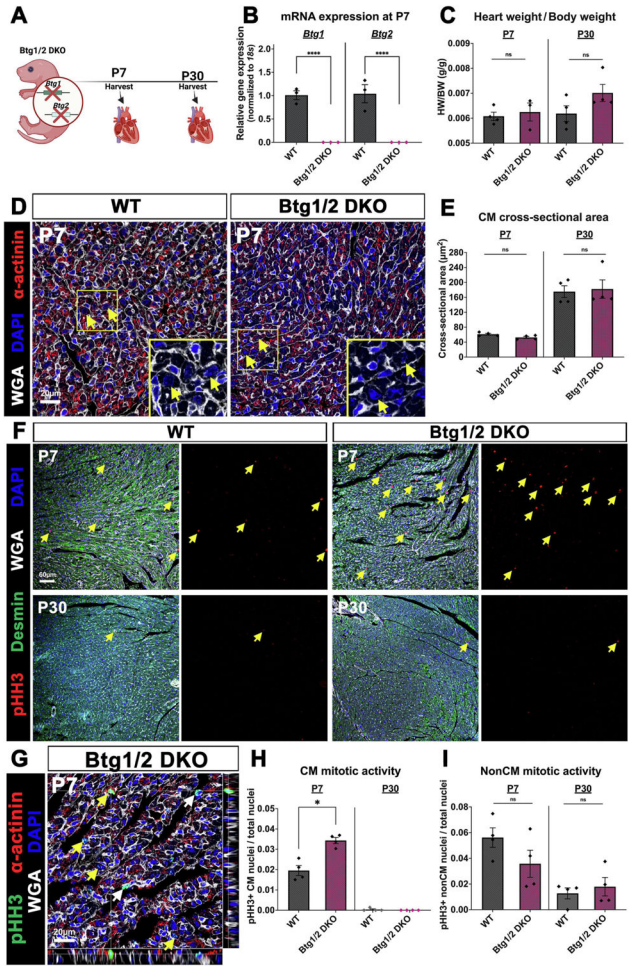


**Figure 2. Constitutive Btg1 and Btg2 double knockout (Btg1/2 DKO) mice exhibit increased cardiomyocyte mitotic activity at P7.**

**(A)** Schematic of postnatal cardiac stages analyzed in Btg1/2 DKO mice. **(B)** RT-qPCR analysis of *Btg1* and *Btg2* gene expression in Btg1/2 DKO mouse ventricular mRNA, with fold change relative to age-matched Wildtype (WT) controls from the same background as Btg1/2 KO. Data are mean ± SEM, with ****p<0.0001 determined by Welch's t test following Shapiro-Wilk test for normal distribution, in n=3 mice per group. **(C)** Heart weight-to-body weight ratios (HW/BW) at P7 and P30 in Btg1/2 DKO mice (n=3 mice at P7, n=4 mice at P30), compared to WT controls (n=4 mice per stage). Data are mean ± SEM, with *p<0.05 determined by Mann Whitney U Test. **(D)** Representative images of cardiac cross-sections at P7 stained with sarcomeric α-actinin and DAPI, with cardiomyocyte cell boundaries identified by WGA. Yellow arrows indicate cardiomyocytes in cross-section, in WT and Btg1/2 DKO mice. Inset images show WGA and DAPI channels for visualization of cell boundaries. **(E)** Quantification of cardiomyocyte (CM) cross-sectional area ($\mu m^2$) in paraffin sections by manual cell tracing based on WGA staining. **(F)** Representative images of Phosphohistone-H3 (pHH3) immunostaining for mitotic activity in neonatal WT and Btg1/2 DKO heart tissues. Yellow arrows indicate increased pHH3 expression at P7 in Btg1/2 DKO mice compared to WT. **(G)** Representative image of Z-stack planes utilized to identify pHH3+ cardiomyocytes (yellow arrows) in all cohorts,

Author Manuscript Author Manuscript Author Manuscript Author Manuscript

with sarcomeres stained by α-actinin. White arrows indicate pHH3+ non-cardiomyocytes, identified by WGA staining without α-actinin expression. **(H)** Cardiomyocyte (CM) mitotic activity measured as ratio of pHH3+ cardiomyocyte nuclei to total DAPI+ nuclei at P7 and P30 in WT and Btg1/2 DKO mouse left ventricles. **(I)** Non-cardiomyocyte (NonCM) mitotic activity is shown as the ratio of pHH3+ non-cardiomyocyte nuclei to total DAPI+ nuclei at P7 and P30 in WT and Btg1/2 DKO mouse left ventricles. For Panels D–I, data are mean ± SEM, with *$p<0.05$ determined by Mann Whitney U Test, in n=4 mice per group, with 2–3 tissue slices analyzed per heart.

Author Manuscript Author Manuscript Author Manuscript Author Manuscript

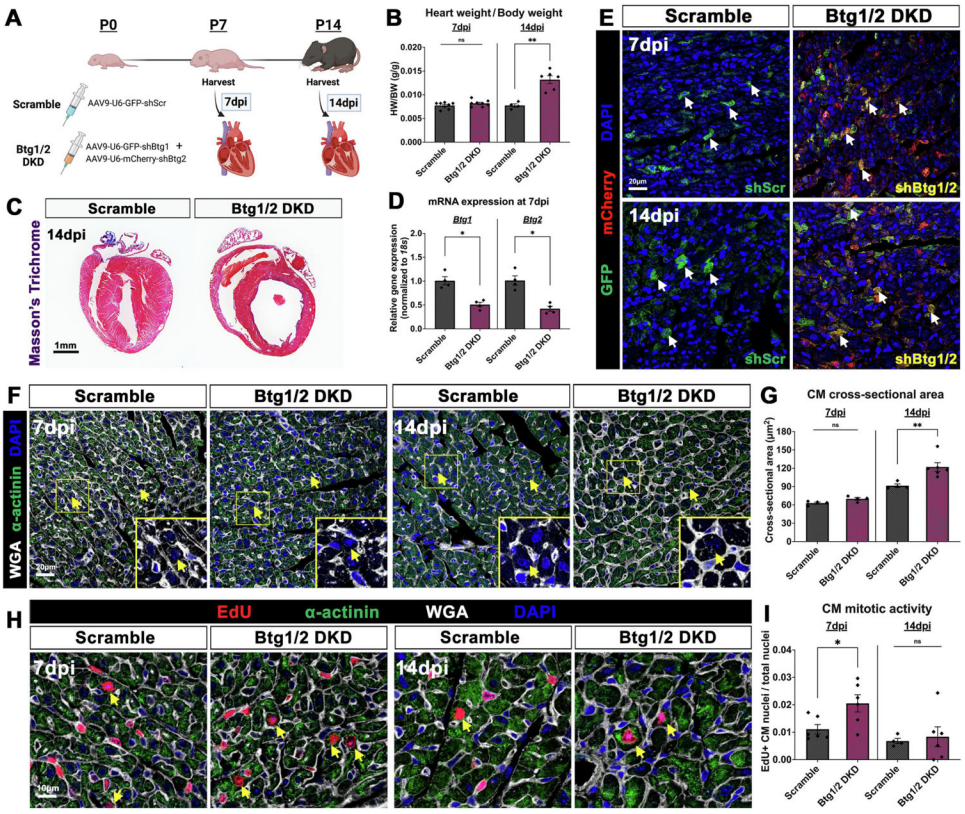


**Figure 3. AAV9-mediated double knockdown of Btg1 and Btg2 (Btg1/2 DKD) in neonatal mice promotes cardiomyocyte cell cycle activity at P7 but causes left ventricular hypertrophy by P14.**

**(A)** Schematic of experimental design for Btg1/2 DKD via AAV9 injections in neonatal C57BL/6 mice. **(B)** Heart weight-to-body weight ratios (HW/BW) at 7- and 14-days post-injection (7dpi and 14dpi respectively), in Btg1/2 DKD mice (n=8 mice at 7dpi, n=6 mice at 14dpi) compared to littermate Scramble-injected controls (n=8 mice at 7dpi, n=4 mice at 14dpi). **(C)** Representative Masson's Trichrome staining of whole heart paraffin sections of Btg1/2 DKD mice at 14dpi compared to Scramble (n=4 mice per group). **(D)** RT-qPCR analysis of *Btg1* and *Btg2* gene expression in Btg1/2 DKD mouse ventricular mRNA at 7dpi, with fold change relative to littermate Scramble-injected controls (n=4 mice per group). **(E)** Representative images of GFP (shScramble or shBtg1) and mCherry (shBtg2) expression to visualize AAV9 transduction in mouse ventricular tissue at 7dpi and 14dpi (n=4 mice per group). White arrows indicate AAV9-mediated reporter gene expression in cardiac muscle. **(F)** Representative images of Scramble and Btg1/2 DKD mouse heart sections stained with WGA, α-actinin, and DAPI. Yellow arrows indicate cardiomyocytes in cross-section. Inset images show WGA and DAPI immunostaining channels only for visualization of cell boundaries. **(G)** Quantification of cardiomyocyte (CM) cross-sectional area ($\mu m^2$) in paraffin sections of Scramble (n=4 mice at 7dpi, n=4 mice at 14dpi) and Btg1/2 DKD (n=4 mice at 7dpi, n=6 mice at 14dpi) mice, by manual cell tracing based on WGA staining, with 2–3 tissue slices analyzed per heart. **(H)** Representative images of EdU incorporation assay for mitotic activity at 7dpi and 14dpi in Btg1/2 DKD and Scramble heart tissues. Yellow arrows indicate EdU+ cardiomyocytes, identified by co-staining with sarcomeric α-actinin and WGA. **(I)** Cardiomyocyte (CM) mitotic activity measured as ratio

Author Manuscript Author Manuscript Author Manuscript Author Manuscript

of EdU+ cardiomyocyte nuclei to total nuclei in Btg1/2 DKD (n=6 mice at 7dpi, n=6 mice at 14dpi) mouse left ventricles compared to Scramble (n=6 mice at 7dpi, n=4 mice at 14dpi), with 3 tissue slices analyzed per heart. Data are mean ± SEM, with *p<0.05, **p<0.01 determined by Mann Whitney U Test.

Author Manuscript
Author Manuscript
Author Manuscript
Author Manuscript



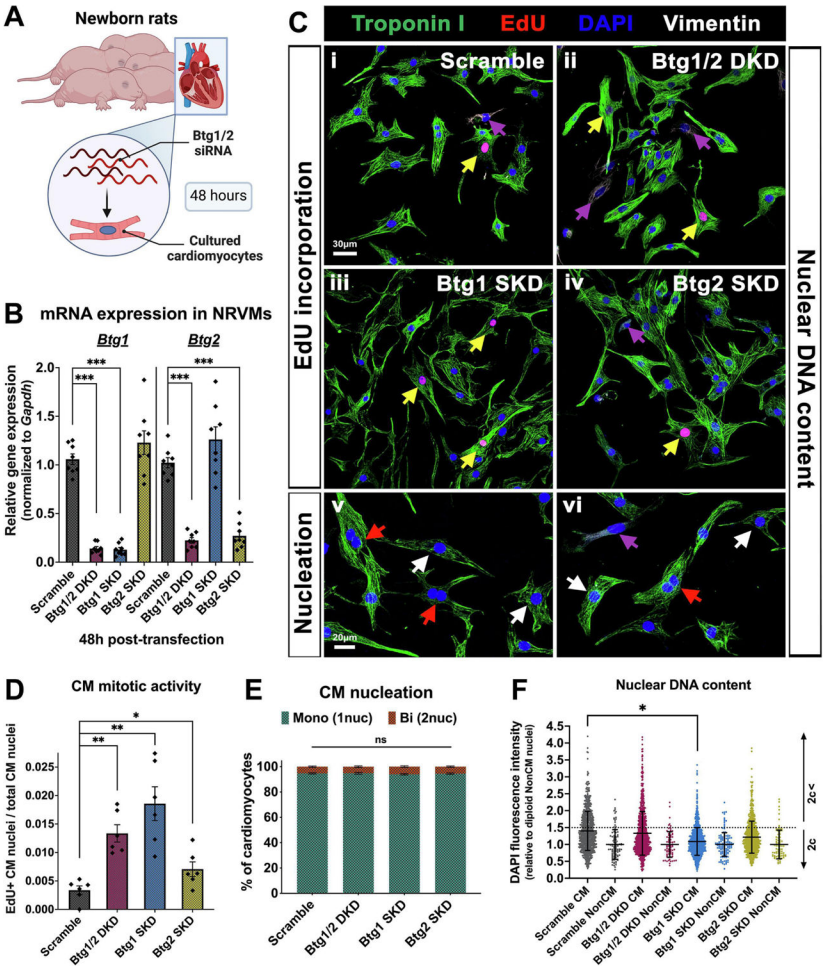


**Figure 4. Btg1/2 depletion via siRNA increases cardiomyocyte proliferation in neonatal rat cultured cardiomyocytes.**

**(A)** Schematic of experimental design for siRNA-mediated knockdown of Btg1/2 in cultured cardiomyocytes from newborn Sprague Dawley rats. **(B)** RT-qPCR analysis of *Btg1* and *Btg2* gene expression with siRNA-mediated Btg1/2 single- (SKD) and double- (DKD) knockdown, relative to Scramble-treated controls, in cultured neonatal rat ventricular cardiomyocytes (NRVM) at 48 hours post-transfection (n=8 culture wells per group). **(C)** Representative images of siRNA-treated NRVMs with Troponin I (green stain) for cardiomyocytes, Vimentin (white stain, purple arrows) for non-cardiomyocytes, and DAPI (blue stain) for nuclei, showing **(i - iv)** EdU incorporation (yellow arrows) for cardiomyocyte mitotic activity, and **(v & vi)** mononucleated (white arrows) and binucleated (red arrows) cardiomyocytes for nucleation counts (n=6 culture wells per group). **(D)** Cardiomyocyte (CM) mitotic activity measured as ratio of EdU+ cardiomyocyte nuclei to total cardiomyocyte nuclei in Btg1/2 DKD and SKD groups compared to Scramble (n=6 culture wells per group, with at least 6 regions per culture well analyzed). **(E)** Percent of total cardiomyocytes exhibiting mono- vs. bi-nucleation in Btg1/2 knockdown groups compared to Scramble, calculated by manual nucleation counts of approximately 3500 CMs from n=6 culture wells per group. Data are mean ± SEM, with *p<0.05, **p<0.01, ***p<0.001 determined by Pairwise Mann Whitney U Tests with respect to Scramble

Author Manuscript Author Manuscript Author Manuscript Author Manuscript

control. (F) DAPI fluorescence intensities were calculated per image for cardiomyocyte (CM) nuclei identified by sarcomeric Troponin I, relative to non-cardiomyocyte (NonCM) nuclei identified by Vimentin. Thresholds for diploid (2c) and polyploid (2c<) nuclear intensities were determined based on standard deviation of NonCM nuclear intensities set as diploid control. Approximately 1000 CM nuclei and 100 NonCM nuclei were analyzed from n=4 culture wells per group. Data are mean ± SD, with *$p<0.05$ determined by Dunn's Kruskal-Wallis Multiple Comparisons Tests with respect to Scramble control. At least two separate cardiomyocyte preparations were utilized for n=4–8 independent culture wells per group for all experiments.

Author Manuscript Author Manuscript Author Manuscript Author Manuscript

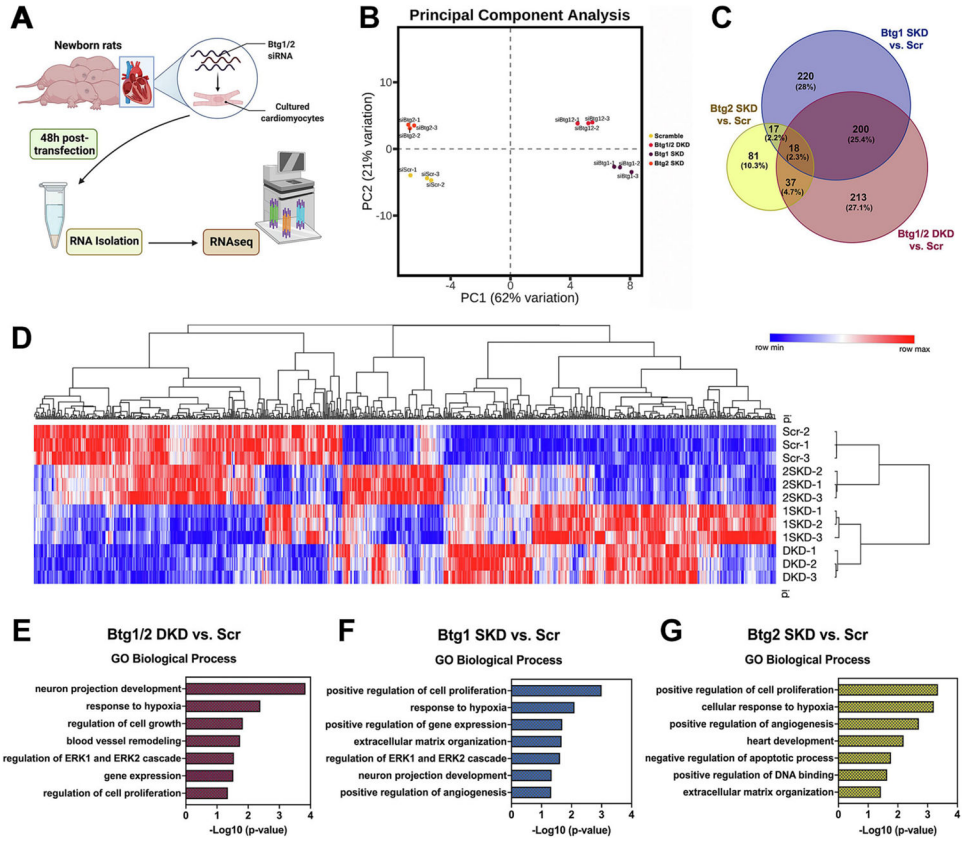


**Figure 5. Transcriptomic profiling by RNAseq indicate significant changes in cell proliferative and hypoxia response signaling in Btg1/2-depleted neonatal rat ventricular myocyte cultures compared to Scramble.**

**(A)** Schematic of RNAseq experimental design for gene expression profiling of Btg1/2 siRNA-treated compared to scramble control cultured rat cardiomyocytes. **(B)** Principal component (PC) analysis shows clustering of biological replicates (n=3 per group) within each siRNA-treated experimental group. **(C)** Venn intersection analysis shows overlap of significantly differentially expressed genes in Btg1/2 single- (Btg1 SKD, Btg2 SKD) and double- (Btg1/2 DKD) knockdown groups compared to Scramble control. **(D)** Heatmap showing 786 significantly differentially expressed genes in Btg1 SKD, Btg2 SKD, and Btg1/2 DKD groups compared to Scramble. **(E)** Gene ontology analysis for significant Biological Process (GO-BP) terms. Histograms show selected top GO-BP terms for significantly differentially expressed genes in Btg1/2 DKD compared to Scramble. **(F)** Selected top GO-BP terms for significantly differentially expressed genes in Btg1 SKD compared to Scramble. **(G)** Selected top GO-BP terms for significantly differentially expressed genes in Btg2 SKD compared to Scramble.